Reliability-Based Design for External Stability of Narrow Mechanically Stabilized Earth Walls: Calibration from Centrifuge Tests

Kuo-Hsin Yang[1]; Jianye Ching, M.ASCE[2]; and Jorge G. Zornberg, M.ASCE[3]

Abstract: A narrow mechanically stabilized earth (MSE) wall is defined as a MSE wall placed adjacent to an existing stable wall, with a width less than that established in current guidelines. Because of space constraints and interactions with the existing stable wall, various studies have suggested that the mechanics of narrow walls differ from those of conventional walls. This paper presents the reliability-based design (RBD) for external stability (i.e., sliding and overturning) of narrow MSE walls with wall aspects L/H ranging from 0.2 to 0.7. The reduction in earth pressure pertaining to narrow walls is considered by multiplying a reduction factor by the conventional earth pressure. The probability distribution of the reduction factor is calibrated based on Bayesian analysis by using the results of a series of centrifuge tests on narrow walls. The stability against bearing capacity failure and the effect of water pressure within MSE walls are not calibrated in this study because they are not modeled in the centrifuge tests. An RBD method considering variability in soil parameters, wall dimensions, and traffic loads is applied to establish the relationship between target failure probability and the required safety factor. A design example is provided to illustrate the design procedure. **DOI: 10.1061/(ASCE)GT.1943-5606.0000423.** © *2011 American Society of Civil Engineers.*

CE Database subject headings: Earth pressure; Centrifuge models; Walls; Soil structures; Calibration.

Author keywords: Narrow MSE wall; Reduced earth pressure; External stability; Reliability-based design; Centrifuge tests.

Introduction

The increase of traffic demands in urban areas has led to the widening of existing highways. A possible solution to increase right of way is to build mechanically stabilized earth (MSE) walls adjacent to existing stabilized walls. Owing to the high cost of additional rights-of-way and limited space available at jobsites, construction of those walls is often done under a constrained space. This leads to MSE walls narrower than those in current design guidelines. Narrow MSE walls are referred to as MSE walls having an aspect ratio L/H (ratio of wall width L to wall height H) of less than 0.7, the minimum value suggested in Federal Highway Administration (FHwA) MSE-wall design guidelines (Elias et al. 2001).

An illustration of narrow MSE walls is shown in Fig. 1, whereas Fig. 2 shows a picture of a narrow MSE wall under construction to increase the traffic capacity in Highway Loop 1 (dubbed "Mopac") in Austin, Texas. In this case, the construction space is limited by a recreational park in close proximity to Highway Loop 1. Narrow MSE walls may also be required when roadways are repaired and extended because of natural and environmental constraints in mountain terrain. The behavior of narrow walls differs from that of conventional walls because of constrained space and interactions with the existing stable wall. Possible differences include the magnitude of earth pressures, location of failure planes, and external failure mechanisms.

Elias et al. (2001) presented design methods for internal and external stabilities of conventional MSE walls in FHwA design guidelines. A factor of safety, FS, is assigned for each mode of failure. The factor of safety must be larger than 1.0 (e.g., $FS_s = 1.5$ against sliding and $FS_o = 2.0$ against overturning) to account for uncertainties in design methods, as well as in soil and material properties. Chalermyanont and Benson (2004, 2005) developed reliability-based design (RBD) methods for internal and external stabilities of conventional MSE walls using Monte Carlo simulations (MCS). In the FHwA design guidelines for shored mechanically stabilized earth (SMSE) wall systems (Morrison et al. 2006), design methods were proposed specifically for wall aspect ratios ranging from 0.3 to 0.7. A minimum value of $L/H = 0.3$ was recommended for constructing narrow walls. The FHwA SMSE design guidelines dealt with uncertainties of narrow walls by increasing the factor of safety rather than considering the actual characteristics of narrow walls.

This study intends to improve previous works by proposing a reliability-based external stability model that realistically considers the effect of reduced earth pressure in narrow walls. The earth pressure of a narrow MSE wall can sometimes be significantly less than that of a conventional wall; therefore, a reduction factor for the earth pressure depending on the design dimension should be taken for narrow walls for more accurate and cost effective design. However, this reduction factor is quite uncertain. A highlight of this paper is therefore to identify the possible value of the reduction factor using a series of centrifuge tests conducted by Woodruff (2003): the probability distribution of the reduction factor is obtained through a Bayesian analysis on the centrifuge test data. This distribution characterizes the possible value of the reduction factor

[1]Assistant Professor, Dept. of Construction Engineering, National Taiwan Univ. of Science and Technology, Taipei, Taiwan. E-mail: khy@mail.ntust.edu.tw

[2]Associate Professor, Dept. of Civil Engineering, National Taiwan Univ., Taipei, Taiwan (corresponding author). E-mail: jyching@gmail.com

[3]Associate Professor, Dept. of Civil Engineering, The Univ. of Texas at Austin. E-mail: zornberg@mail.utexas.edu
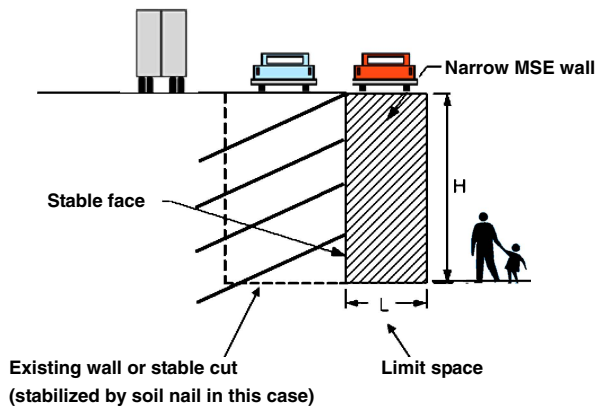
Fig. 1. Illustration of a narrow MSE wall

Fig. 2. Construction of a narrow MSE wall at Highway Loop 1 in Austin, Texas: (a) front view; (b) overview

conditioning on the centrifuge tests and is later used to develop RBD charts for narrow MSE walls. The proposed RBD charts will allow designers to evaluate the external stability by considering various design variables of the wall system (e.g., soil parameters, wall dimensions, and traffic loads). Readers should notice that MSE walls in this study are assumed to be built under good design practice (i.e., no accumulation of water pressure within MSE walls because cohesionless materials were used as backfill and drainage devices were properly installed). When a wall is not constructed carefully, water pressure may not dissipate easily; therefore, the design charts proposed in this study may not be proper. However, this study does not intend to address this scenario. In addition, the

focus of this study is on the sliding and overturning failure model of external stability. The bearing capacity failure mode of external stability is not calibrated in this study because it is not modeled in the centrifuge tests.

This paper is organized into two parts. In the first part, external stability of narrow MSE walls is investigated in a deterministic manner. Definition of the external stability model considering the reduction factor is introduced. In the second part, external stability is reevaluated using a probabilistic approach. The probability distribution of the reduction factor for earth pressure is obtained, based on Bayesian analysis, from centrifuge test data on narrow walls. A simplified RBD method is applied to establish the relation between target failure probabilities and required nominal safety ratios. This relation allows designers to achieve a RBD by using a safety-factor approach. A design example to illustrate the design procedure will also be demonstrated.

Background and Characteristics of Narrow MSE Wall System

The behaviors of narrow walls are different from those of conventional walls because of constrained space and interaction with stable walls. Such differences include the magnitude of earth pressures, the location of failure planes and the external failure mechanisms. A brief discussion of those differences and background information are given as follows.

Magnitude of Earth Pressure

Earth pressure of narrow walls has been studied by several researchers by centrifuge tests (Frydman and Keissar 1987; Take and Valsangkar 2001), by limit equilibrium analyses (Leshchinsky et al. 2004; Lawson and Yee 2005) and by finite-element analyses (Kniss et al. 2007; Yang and Liu 2007). Frydman and Keissar (1987) conducted centrifuge tests to investigate the earth pressure on retaining walls near rock faces in both at-rest and active conditions. They found that the measured earth pressure decreases with increasing depth. Take and Valsangkar (2001) performed a series of centrifuge tests on narrow walls and observed similar phenomenon of reduced earth pressure.

Leshchinsky et al. (2004) performed a series of limit equilibrium analyses on MSE walls with limited space between the wall and stable face. They showed that as the aspect ratio decreases, the earth pressure also decreases, most likely because potential failure surfaces could form in the restricted space. Lawson and Yee (2005) used an approach similar to Leshchinsky et al. (2004) to develop design charts for the earth pressure coefficients. They showed that the forces are less than those for active earth pressures and decrease as the aspect ratio decreases.

Kniss et al. (2007) and Yang and Liu (2007) conducted a series of finite-element analyses to evaluate the effect of wall aspect ratios on reduced earth pressures. Finite-element analyses reported the earth pressures along two vertical profiles: along the vertical edge (external earth pressure) and the along the vertical center profile (internal earth pressure). Fig. 3 shows the results from finite-element and limit equilibrium analyses under active conditions. The earth pressure calculated by limit equilibrium analyses is in between the internal and external earth pressures (i.e., average earth pressure) because the critical failure surface passes through the entire reinforced soil wall. The presented "normalized" earth pressure coefficients R_d (normalized by the Rankine one) show a clear evidence of reduction with decreasing L/H.

In summary, all aforementioned research concluded that earth pressure for narrow walls is less than that calculated using the
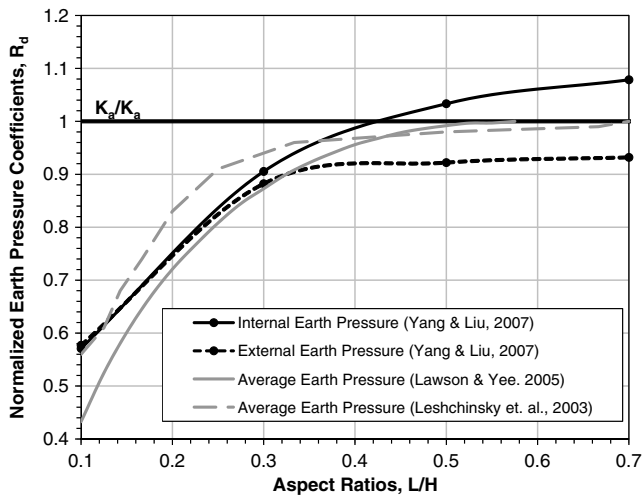
Fig. 3. Reduced earth pressure coefficients at different vertical profiles

conventional (Rankine) earth pressure equation. Furthermore, the reduction will become pronounced with (1) increasing depth and (2) decreasing wall aspect ratio. This observation implies that designs with the conventional earth pressure may be conservative for narrow walls.

The reduction of earth pressure observed in past studies as well as in Fig. 3 is mainly attributable to the combination of two mechanisms: arching effect and boundary constraint. Arching effect is a result of soil-wall interaction. Soil layers settle because of their self weights, and simultaneously, the wall provides a vertical shear fric-

tional force to resist the settlement. This vertical shear force reduces the overburden pressure and, consequently, reduces the lateral earth pressure (e.g., Handy 1985; Filz and Duncan 1997a, b). Further, Yang and Liu (2007) found the effect of arching effect on reduced earth pressure is less prominent under active conditions. This is because the movement of the wall face attenuates the effect of soil-structure interaction under active conditions. Compared with the arching effect that influences the earth pressure along the soil-wall interface, the boundary constraint is a kinematics constraint on the overall failure mechanism. Its effect is likely to place a limit to prevent the full development of potential failure surfaces. As a result, the size and weight of the failure wedge within narrow walls is less than that within conventional walls, and so are the earth pressures within narrow walls.

Location of Failure Plane

Woodruff (2003) performed a series of centrifuge tests on reinforced soil walls adjacent to a stable face. The test scope is summarized in Table 1. The tests were undertaken on 24 different walls with L/H ranging from 0.17 to 0.9. All the reduced-scale walls were 230 mm tall and the wall facing batter was 11 vertical to 1 horizontal. Monterey No. 30 sand was used as the backfill material. The unit weight is around 16.05 kN/m^3 and the friction angle is 36.7º interpolated from a series of triaxial compression tests (Zornberg 2002) at the targeted backfill relative density of 70%. The reinforcements used in the centrifuge study are nonwoven geotextiles with the following two types: Pellon True-grid and Pellon Sew-in. Pellon True-grid is composed of 60% polyester and 40% rayon fabric. The fabric, tested by wide-width-strip tensile tests (ASTM 2009), has a strength of 0.09 kN/m in the machine

Table 1. Summary of Woodruff's Centrifuge Test Parameters

Test		Aspect ratio (L/H)	Reinforcement type	Reinforcement vertical spacing (mm)	Failure mode	g-level at failure
1	a	0.9	R1	20	Internal	18
	b	0.6	R1	20	Compound	17
2	a	0.6	R2	20	Compound	39
	b	0.4	R2	20	Compound	41
3	a	0.7	R2	20	Internal	38
	b	0.7	R2	20	Internal	49
	c	0.7	R2	20	Internal	47
	d	0.7	R2	20	Internal	44
4	a	0.7	R4	20	None	None
	b	0.5	R4	20	None	None
	c	0.3	R4	20	None	None
	d	0.3	R4	20	None	None
5	a	0.17	R4	20	Overturning	7
	b[a]	0.2	R4	20	None	None
	c	0.25	R4	20	Overturning	32
	d[a]	0.2	R4	20	None	None
6	a[b]	0.3	R4	20	None	None
	b[c]	0.3	R4	20	None	None
	c[d]	0.2-0.3	R4	20	Overturning	78
	d	0.3	R4	20	None	None
7	a	0.25	R4	10	Overturning	38
	b	0.25	R4	30	Overturning	2.5
	c	0.25	R4	40	Overlap Pullout	1
	d	0.25	R4	50	Overlap Pullout	1

[a]Test 5b and Test 5d have reinforcement configurations wrapped around at the interface between the reinforced soil wall and stable face.
[b]Test 6a has a top reinforcement configuration attached to a stable face.
[c]Test 6b has a top reinforcement configuration wrapped around at the interface between the reinforced soil wall and stable face.
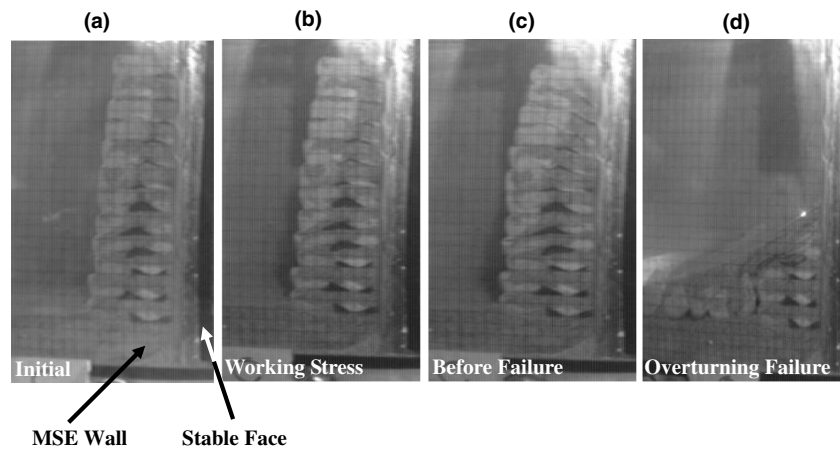[d]Test 6c has an inclined wall face.

Fig. 4. Photographic images from centrifuge: (a) initial condition (1 g); (b) working stress (10 g); (c) right before failure (32 g); (d) failure condition (32 g)

direction and 1.0 kN/m in the transverse direction (referred to as R2 and R4, respectively, in Table 1). Pellon Sew-in is made of 100% polyester fabric. The fabric has a strength of 0.03 kN/m in the machine direction and 0.1 kN/m in the transverse direction (referred to as R1 and R3, respectively, in Table 1). The model walls were placed in front of an aluminum strong box that simulates the stable face. Woodruff (2003) loaded each wall to failure and recorded the load (acceleration g force) required to fail the wall. Fig. 4 shows a series of responses observed from Test 5c ($L/H = 0.25$).

Woodruff (2003) observed that when $L/H > 0.6$, the wall fails in an internal mode with weaker reinforcement (Pellon Sew-in) or no failure with stronger reinforcement (Pellon True-grid). If a wall fails, the critical failure plane is linear and passes through the entire reinforced area. When L/H is between 0.25 and 0.6, the wall fails internally in a compound mode with bilinear failure surfaces that pass through the reinforced soil and the edge between the reinforced backfill and stable wall. The inclination angle of the failure plane in a compound mode is less than that predicted by the Rankine theory. However, these are more relevant to internal stability and are not relevant to this study.

External Failure Mechanism

Woodruff (2003) also observed that when L/H decreases below 0.25, the failure mode changes from internal to external: such walls all fail externally in an overturning mode independent of the strength of reinforcement. The external failure is initiated from a "gap" (or separation) at the edge between the reinforced backfill and stable wall [see Fig. 4(c)]. This gap tends to pull the MSE wall away from the stable wall, resulting in overturning failure. Yang et al. (2008) performed finite-element analyses to investigate the mechanics of this gap and concluded that the gap is actually a zero pressure zone, a zone without normal earth pressure acting to the narrow wall, at the moment of wall failure. The length of the zero

pressure zone grows with decreasing L/H and reaches approximately 85% of the wall height at $L/H = 0.25$. Yang et al. (2008) recommended several means to prevent the development of the zero pressure zone to improve the external stability of narrow walls. The dominant failure modes and current design methods with various aspect ratios are summarized in Table 2.

Deterministic Analyses–External Stability Model

Although both internal and external stabilities are important subjects for the design of narrow walls, this paper focuses on the external stability of narrow MSE walls, specifically for the sliding and overturning failure mode. The internal stability (e.g., the compound failure mode in Table 2) is not considered in this paper owing to the lack of mature models, which are typically required for calibrating design factors. As for the bearing-capacity failure mode in external stability, it is not seriously considered in this paper for the following reason. One limitation of the series of tests performed by Woodruff is that a rigid boundary was placed below the narrow wall. This rigid boundary prohibits the bearing capacity failure. As a result, even if the bearing capacity mode is considered, it is impossible to be calibrated by using the centrifuge test results. Yet, based on noncalibrated simulations, it is found that for MSE walls with L/H greater than 0.35, the failure probability for this mode is usually less than 0.01. For walls with L/H less than 0.35, it is advisable that the bearing capacity mode should be carefully assessed. Readers interested in RBD for the internal stability and bearing capacity mode for conventional MSE walls are referred to Chalermyanont and Benson (2004, 2005).

The forces acting on a narrow MSE wall are shown in Fig. 5. The length of reinforcement often covers the entire width of the wall, so L is typically equal to the length of reinforcement. The total weight W of backfill can be computed using Eq. (1):

Table 2. Summary of Wall Failure Modes and Corresponding Design Guidelines

Wall aspect ratio	$L/H < 0.25$	$0.25 < L/H < 0.3$	$0.3 < L/H < 0.6$	$0.6 < L/H < 0.7$	$L/H > 0.7$
Failure mode	External	Compound[a]		Internal	
Design method	Cement-stabilized wall[b]		FHwA SMSE-wall design guidelines (Morrison et al. 2006)	FHwA MSE-wall design guidelines (Elias et al. 2001)	

[a]The compound failure has a failure surface formed partially through the reinforced soil and partially along the interface between the MSE and stabilized wall faces.
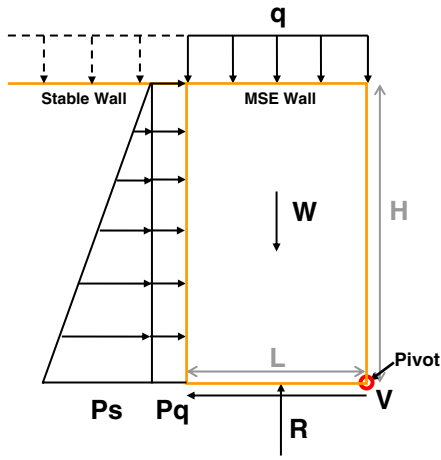[b]A cement-stabilized wall is suggested by the reinforced earth company.

Fig. 5. Forces acting on a narrow MSE wall

$$W = \gamma \cdot L \cdot H \qquad (1)$$

where γ = unit weight of backfill; L = wall width; and H = wall height.

The traffic load is modeled as an uniform surcharge pressure q. The magnitude of the minimum traffic loads suggested by AASHTO (2002) is equivalent to 0.6 m (2 ft) height of soil over the traffic lanes. Therefore, q is expressed as Eq. (2):

$$q = 0.6 \cdot \gamma \,(\text{SI Unit}) \quad \text{or} \quad q = 2 \cdot \gamma \,(\text{English Unit}) \qquad (2)$$

The resulting vertical component is expressed as R. As suggested in FHwA (Elias et al. 2001) and AASHTO (2002) design guidelines, designs should not rely on live loads as a part of resisting force/moment; therefore, R is equal to W, regardless of q. V is the shear resistance along the bottom of the wall and evaluated using Eq. (3):

$$V = R \cdot \tan\delta = W \cdot \tan\delta \qquad (3)$$

where δ = interface friction angle between foundation and reinforcement, taken to be 2/3 of the friction angle of the foundation soil ϕ_f.

The lateral earth pressures attributable to the backfill weight and traffic load are denoted by P_s and P_q, respectively. They can be calculated using Eq. (4)

$$P_s = \frac{1}{2}\gamma \cdot H^2 \cdot K_a \cdot (1 - F) \qquad (4)$$

and Eq. (5)

$$P_q = q \cdot H \cdot K_a \cdot (1 - F) \qquad (5)$$

where $K_a = \tan^2(45 - \phi/2)$ = conventional active earth-pressure coefficient from the Rankine theory; and F = reduction factor, addressing the reduction of earth pressure in narrow walls, as discussed in previous sections. The value of F will be discussed in details in the next section. It is clear that F is bounded between 0 and 1. $F = 0$ means no reduction; it often happens at $L/H \geq 0.7$, and $F = 1$ means full reduction or no lateral earth pressure acting on MSE walls. It is also very important to note that these lateral earth thrusts are reactive forces rather than direct forces acting from the stable face to the MSE wall. These reactive forces may be affected by numerous unmodeled effects, such as nonlinear distribution of earth pressure, arching effects, boundary constraints, and spatial variability. It is highly unlikely that the Rankine theory is able to fully capture these complexities. Because separate treatment of all model uncertainties is not possible, the reduction factor

F is employed to accommodate these model uncertainties and will be calibrated by using the Bayesian analysis described in the next section.

Last, the cohesion of backfill is not considered because cohesionless materials are advised for backfill (Elias et al. 2001; AASHTO 2002). In addition, the water pressure is also not included in the stability mode. This is because if a MSE wall is constructed carefully by following guidelines (Elias et al. 2001; AASHTO 2002), water pressure can be minimized by taking the following actions:

- Cohesionless materials are commonly recommended as backfills in current design guidelines. These materials are highly permeable so that water pressure would not accumulate.
- Installation of drainage pipes, blankets and weep holes is typically required in design guidelines to facilitate drainage.

By treating the reinforced soil wall as a rigid mass, safety ratio against sliding (SR_s) and overturning (SR_o) can be calculated as Eq. (6)

$$SR_s = \frac{\Sigma \text{ horizontal resisting forces}}{\Sigma \text{ horizontal driving forces}} = \frac{W \tan\delta}{P_s + P_q}$$
$$= \frac{\gamma \cdot L/H \cdot \tan(2\phi_f/3)}{[\gamma/2 + q/H] \cdot \tan^2(45 - \phi/2)} \cdot \frac{1}{1 - F} \qquad (6)$$

and Eq. (7)

$$SR_o = \frac{\Sigma \text{ resisting moments}}{\Sigma \text{ driving moments}} = \frac{W \cdot L/2}{P_s \cdot H/3 + P_q \cdot H/2}$$
$$= \frac{\gamma \cdot (L/H)^2}{[\gamma/3 + q/H] \cdot \tan^2(45 - \phi/2)} \cdot \frac{1}{1 - F} \qquad (7)$$

In Eqs. (4) and (5), a linear earth pressure distribution is assumed for P_s and a uniform earth pressure distribution is assumed for P_q. In fact, the reduced earth pressure is nonlinearly distributed with wall height. This deviation in the magnitude of total earth pressure induced by the more realistic nonlinear distribution is quantified as part of the model uncertainty by the reduction factor F. Also, the length of moment arm in Eq. (7) induced by the more realistic nonlinear distribution is not much different from that by assuming linear earth pressure distribution. Based on the results from this study, the length of moment arm for P_s for nonlinear cases is approximately 0.338H (height) for walls with $L/H = 0.3$ and decreases to approximately 0.333H for walls with $L/H = 0.7$, both fairly close to $H/3$ for the linear distribution case.

The safety ratios calculated by Eqs. (6) and (7) are uncertain (or random) because the soil properties (e.g., friction angle) and F are uncertain. The nominal safety ratios for the two modes, denoted by $\overline{SR}_s$ and $\overline{SR}_o$, are taken to be Eq. (8)

$$\overline{SR}_s = \frac{\bar{\gamma} \cdot L/H \cdot \tan(2\bar{\phi}_f/3)}{[\bar{\gamma}/2 + \bar{q}/H] \cdot \tan^2(45 - \bar{\phi}/2)} \cdot \frac{1}{1 - \overline{F}} \qquad (8)$$

and Eq. (9)

$$\overline{SR}_o = \frac{\bar{\gamma} \cdot (L/H)^2}{[\bar{\gamma}/3 + \bar{q}/H] \cdot \tan^2(45 - \bar{\phi}/2)} \cdot \frac{1}{1 - \overline{F}} \qquad (9)$$

where $\bar{\gamma}$ = nominal value (e.g., mean value) of γ, and the same notation applies to other variables. If the effect of F is neglected ($F = 0$), Eqs. (8) and (9) turn into the equations for evaluating the external stability of conventional walls.

The rigidity of the wall face is not included in the stability model, which is consistent with the current design guidelines (Elias et al. 2001; AASHTO 2002). The effect of facing rigidity can be

viewed as an additional resisting force/moment. Thus, the method described in this paper is more appropriate for MSE walls with flexible facing. Safety ratios for walls with rigid facing will be larger than (the failure probabilities will be less than) those predicted using the method described herein.

Probability Distribution of Reduction Factor F

Deterministic Estimation of Reduction Factor F

As mentioned earlier, previous research was conducted to investigate the effect of reduction in the lateral earth pressure on narrow walls. Among them, Yang and Liu (2007) performed a finite-element study to quantify the effect of L/H on the reduction of earth pressures. Their numerical models are calibrated using the data from Frydman and Keissar (1987) and Take and Valsangkar (2001) centrifuge tests. Fig. 6 shows the comparisons between the calculated results from Yang and Liu's finite-element analyses (red dots) and the measured data from Frydman and Keissar's centrifuge tests (black squares and white triangles) under the at-rest condition and under the active condition. The data presented in Fig. 6 is a combination of test results of wall models with L/H from 0.1 to 1.1. In Fig. 6, both axes are presented in nondimensional quantities: y-axis presents nondimensional depth z/L, where z is the depth and L is the wall width. Similarly, x-axis presents the nondimensional external earth pressure coefficient k_w', evaluated by lateral earth pressure σ_x normalized by overburden pressure. Also indicated in Fig. 6, $K_o = 1 - \sin\phi$ is Jaky's at-rest earth pressure coefficient.

Fig. 7 presents the comparison between the calculated results (dots) and the measured data from Take and Valsangkar's centrifuge tests (squares) for two different wall widths ($L/H = 0.1$ and 0.55). The comparisons in Figs. 6 and 7 demonstrate consistency between Yang and Liu's calibrated results and the centrifuge tests.

Based on the calibrated finite-element model, Yang and Liu (2007) further performed a series of parametric studies to quantify

the value of the reduced earth pressures for various aspect ratios, locations [vertical edge (external earth pressure) or center of reinforced wall (internal earth pressure)], and stress states (at-rest or active conditions). The results from at-rest condition could be applied to earth pressures for rigid retaining walls or MSE walls with inextensible reinforcements (i.e., metal strip, bar, or mat), while those from active conditions could be applied to earth pressures for flexible retaining walls or MSE walls with extensible reinforcements (i.e., geosynthetics). They concluded that the earth pressures of narrow walls can be estimated by multiplying a factor R_d to the conventional earth pressures, as shown in Eq. (10):

$$P_{L/H<0.7} = P_{L/H>0.7} \cdot R_d(L/H) \qquad (10)$$

where $P_{L/H<0.7}$ is the earth pressure of a narrow MSE wall and $P_{L/H>0.7}$ is the earth pressure of a conventional MSE wall. The estimate for $R_d(L/H)$, later referred to as the nominal value $\bar{R}_d(L/H)$, is shown in Fig. 3 under the active condition. In fact, the reduction factor $F = F(L/H)$ defined previously is exactly $1 - R_d(L/H)$, so the nominal reduction factor becomes Eq. (11):

$$\bar{F}(L/H) = 1 - \bar{R}_d(L/H) \qquad (11)$$

In this study, the reduction factor of the average earth pressure under the active condition is taken since it is commonly chosen in practice for the evaluation of external stabilities, regardless of the rigidity of walls (Elias et al. 2001; AASHTO 2002). The nominal reduction factor $\bar{F}(L/H)$ is obtained by averaging $\bar{R}_d(L/H)$ for external and internal earth pressure in Fig. 3 (i.e., average earth pressure) and converting to $\bar{F}(L/H)$ by Eq. (11). The so-obtained $\bar{F}(L/H)$ is shown in Fig. 8, which shows $\bar{F}(L/H)$ approaches zero when L/H increases toward 0.7 and becomes zero since $L/H > 0.7$. This condition indicates no reduction of earth pressure is necessary for $L/H > 0.7$; consequently, the calculation of earth pressure can continuously transit from narrow walls ($L/H < 0.7$) to conventional walls ($L/H > 0.7$). A polynomial regression equation for the curve in Fig. 8 is given in Eq. (12):

$$\bar{F}(L/H) = \begin{cases} -3.6416 \cdot (L/H)^3 + 6.2285 \cdot (L/H)^2 - 3.6173 \cdot L/H + 0.7292 & \text{for } 0.1 \leq L/H < 0.7 \\ 0 & \text{for } L/H \geq 0.7 \end{cases} \qquad (12)$$

Variability in Reduction Factor: Bayesian Analysis of Centrifuge Test Data

Eq. (12) is just an estimation of the reduction factor as a function of L/H. However, for the purpose of RBD, the variability in $F(L/H)$ that characterizes the model uncertainties should be also taken into account. Centrifuge tests by Frydman and Keissar (1987) and Take and Valsangkar (2001) are insufficient to update the variability in $F(L/H)$ because these tests are mainly focused on the at-rest condition and only a few on the active condition. Compared with these tests, the 24 sets of centrifuge tests on narrow walls performed by

Woodruff (2003) (discussed in the section "Location of Failure Plane") seem to provide much more information. Unlike Frydman and Keissar (1987) and Take and Valsangkar (2001), Woodruff (2003) did not directly measure the earth pressures but only observed the failure patterns. Because there are many tests performed by Woodruff (2003), the amount of information may be sufficient to update the variability of $F(L/H)$ by using Bayesian analysis.

The variability in $F(L/H)$ is quantified through an uncertain scaling factor U: the actual value of $F(L/H)$ is taken to be the best estimate in Eq. (12) scaled by the factor U as shown in Eq. (13)

$$F(L/H, U) = \begin{cases} (-3.6416 \cdot (L/H)^3 + 6.2285 \cdot (L/H)^2 - 3.6173 \cdot L/H + 0.7292) \cdot U & \text{for } 0.1 \leq L/H < 0.7 \\ 0 & \text{for } L/H \geq 0.7 \end{cases} \qquad (13)$$
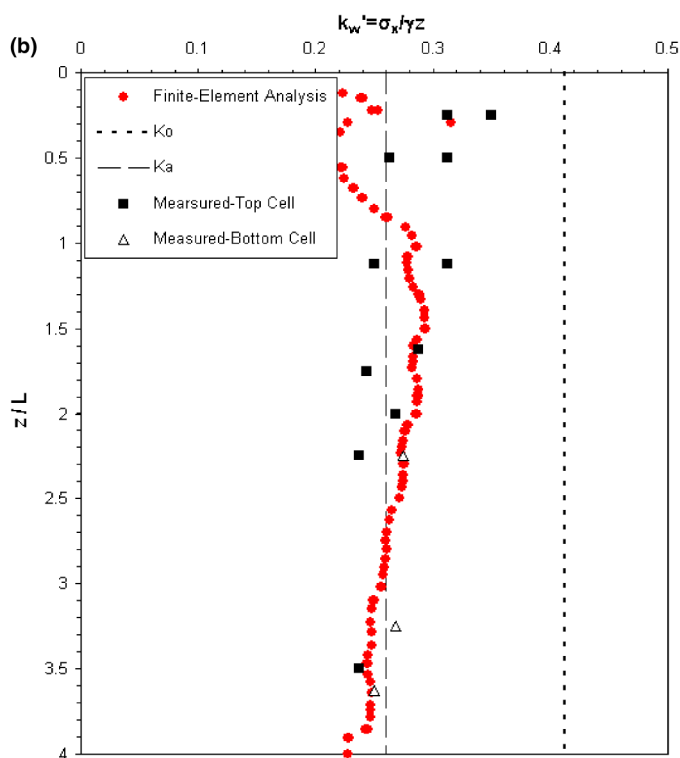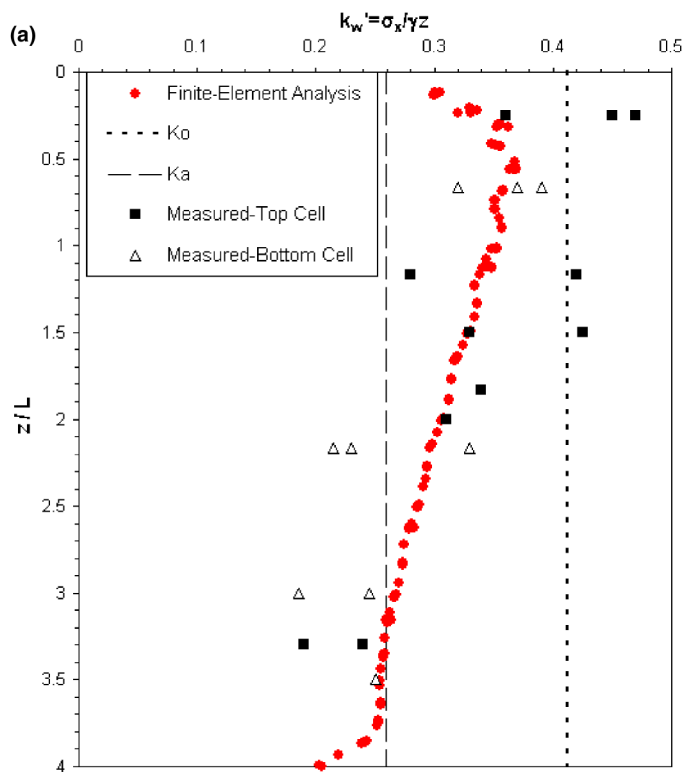
Fig. 6. Comparison of the finite-element analysis performed by Yang and Liu (2007) and Frydman's centrifuge test results: (a) at-rest condition; (b) active condition

Fig. 7. Comparison between the finite-element analysis performed by Yang and Liu (2007) with Take's centrifuge test results

Fig. 8. Nominal reduction factor $\bar{F}(L/H)$ for various aspect ratios

This scaling parameter U is adopted to accommodate model uncertainties, including the possible bias and variability in the reduction factor described by Eq. (12). The prior probability density function (PDF) of U is taken to be uniformly distributed over [0, 2.5] to prevent $F > 1$. Based on Woodruff's test results, the posterior PDF of U can be updated through the Bayesian analysis as shown in Eq. (14):
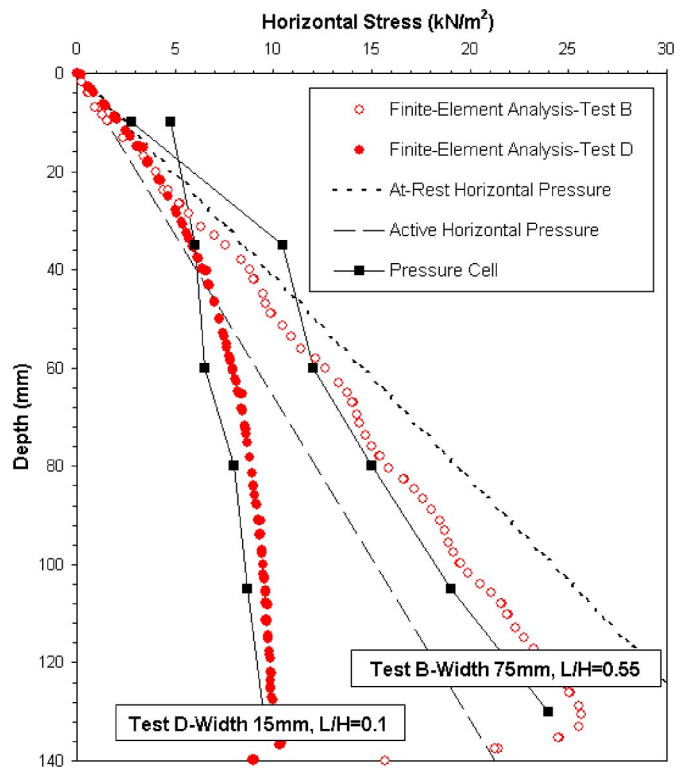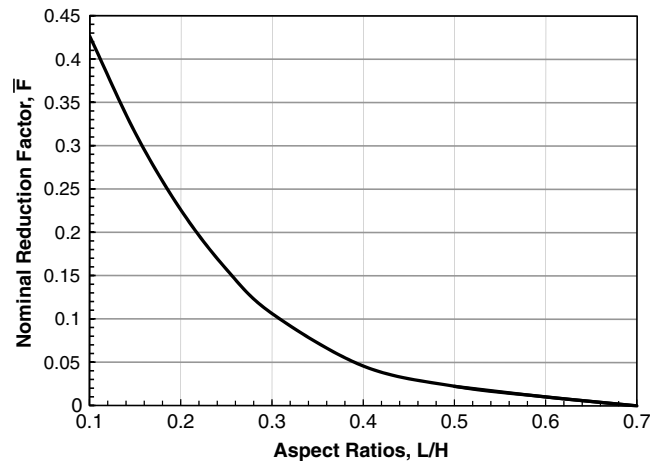
$$f(u|D) = \frac{f(D|u)f(u)}{f(D)} = \frac{\int f(D|u, \phi_{CF})f(\tan \phi_{CF})d\phi_{CF} \cdot f(u)}{f(D)} \quad (14)$$

where $D = \{D_1, \ldots, D_m\}$ = all centrifuge test results (D_j = test result of the jth test); m = total number of tests; $f(u)$ and $f(\tan \phi_{CF})$ = prior PDFs of U and the tangent of the backfill friction angle for the centrifuge tests; $f(u|D)$ = posterior PDF, characterizing the variability of U conditioning on the centrifuge test data; $f(D|u, \phi_{CF})$ = likelihood function; and $f(D)$ = normalizing constant to ensure the integration of $f(u|D)$ is unity.

In Eq. (14), the friction angle ϕ_{CF} is the backfill friction angle in Woodruff's tests. This friction angle is estimated to be 36.7°

interpolated from a series of triaxial compression tests (Zornberg 2002) at the targeted backfill relative density of 70%. Therefore, the PDF $f(\tan\phi_{CF})$ of this friction angle is taken to be normally distributed with mean value = $\tan(36.7°)$ and coefficient of variation (COV) chosen to be 5, 10, 15, and 20%. The COV quantifies the variability in the interpolation process, estimated to be within the range of 5–20%.

To incorporate Woodruff's test results into the Bayesian analysis, the test results are quantified according to the following two principles:

1. If the jth test indicates no failure, D_j contains two types of information: $SR_o > 1.0$ and $SR_s > 1.0$. Therefore, the likelihood function for the jth test should be as calculated in Eq. (15):

$$
\begin{aligned}
f(D_j|u, \phi_{CF}) &= P(SR_o^j > 1 \;\&\; SR_s^j > 1|u, \phi_{CF}) \\
&= I\left(\frac{2 \cdot L/H_j \cdot \tan(2\phi_{CF}/3)}{\tan^2(45 - \phi_{CF}/2)} > 1 - F(L/H_j, u) \right) \\
&\quad \times I\left(\frac{3 \cdot (L/H_j)^2}{\tan^2(45 - \phi_{CF}/2)} > 1 - F(L/H_j, u) \right)
\end{aligned}
\tag{15}
$$

where L/H_j = aspect ratio for the jth test; and $I(\cdot)$ = indicator function. The surcharge term q does not show up here because the surcharge pressure is zero for all tests conducted by Woodruff (2003). The unit weight term γ appears in both nominator and denominator of stability model and is canceled out in Eq. (15); $\phi_f = \phi_{CF}$ is also taken for the foundation soil because Woodruff used the same backfill material for the foundation.

2. If the jth test indicates overturning failure, D_j contains the information that $SR_o < 1.0$. Strictly speaking, this result does not imply $SR_s > 1.0$. Therefore, the likelihood function for the jth test should be as shown in Eq. (16):

$$
\begin{aligned}
f(D_j|u, \phi_{CF}) &= P(SR_o^j < 1|u, \phi_{CF}) \\
&= I\left(\frac{3 \cdot (L/H_j)^2}{\tan^2(45 - \phi_{CF}/2)} < 1 - F(L/H_j, u) \right)
\end{aligned}
\tag{16}
$$

Fig. 9 shows the resulting posterior PDF $f(u|D)$ for various choices of the COV level of $\tan(\phi_{CF})$. The posterior PDF is not very sensitive to the assumed prior COV levels.

In Bayesian analysis, the updating of U may interact with the updating of $\tan(\phi_{CF})$. It is therefore instructive to also illustrate the posterior PDF of $\tan(\phi_{CF})$. Fig. 10 shows the posterior PDFs of $\tan(\phi_{CF})$ when the COV of the prior PDF of $\tan(\phi_{CF})$ is 5, 10, 15, and 20%. The updated PDF of $\tan(\phi_{CF})$ suggests $\tan(\phi_{CF})$ is more likely to be around $\tan(36.5°)$, which is very close to the prior mean value $\tan(36.7°)$.

Reliability-Based Design Calibrated by Centrifuge Test Data

The key contribution of this research is to convey the information learned from the centrifuge tests into guidelines that can be directly implemented to practical designs in the format of RBD. In this section, RBD results calibrated by the centrifuge data will be presented in the form of η^* versus P_F^* relation (η^* is the required nominal safety ratio and P_F^* is the target failure probability), which is
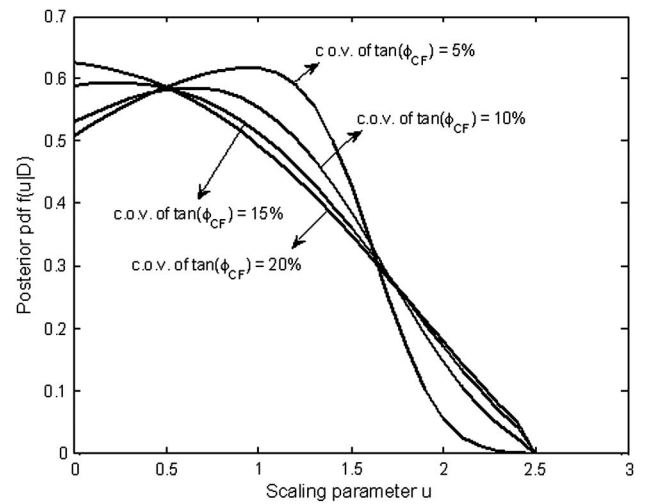

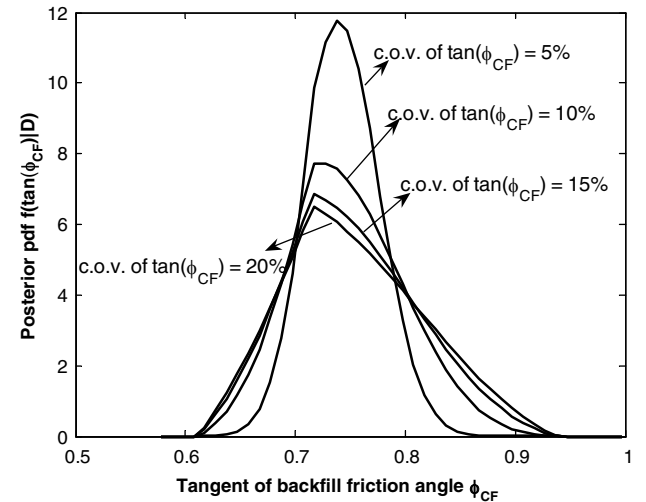**Fig. 9.** Posterior PDFs of U with different assumed COVs of $\tan(\phi)_{CF}$

Fig. 10. Posterior PDFs of $\tan(\phi)_{CF}$ with different assumed COVs of $\tan(\phi)_{CF}$

determined by a simplified RBD method proposed by Ching (2009). The review and validation of this simplified RBD method is presented in the appendix. Once the η^* versus P_F^* relation is obtained, the required nominal safety ratio η^* corresponding to a prescribed target failure probability P_F^* can be readily identified. A design with nominal safety ratio $> \eta^*$ will also satisfy failure probability $< P_F^*$. This method requires the ability to simulate Z samples.

In a typical future design, the random variables Z contain the tangent of backfill friction angle $\tan(\phi)$ (Z_1), tangent of foundation friction angle $\tan(\phi_f)$ (Z_2), unit weight γ (Z_3), traffic load q (Z_4), and scaling parameter U (Z_5). Only U depends on D; the rest are independent of D. Therefore, $\{\tan(\phi), \tan(\phi_f), \gamma, q\}$ samples should be drawn from their prior PDFs, whereas U should be drawn from the posterior PDF $f(u|D)$. The friction angle ϕ here is different from ϕ_{CF} in the previous section; the former is the backfill friction angle in a future design, while the latter is the backfill friction angle used in Woodruff's tests.

Table 3. Assumed Distributions for the Random Variables

	Variables	PDF	μ	COV
Z_1:	$\tan(\phi)$	Normal	$\tan(30°)\sim\tan(45°)$	10%
Z_2:	$\tan(\phi_f)$	Normal	$\tan(30°)\sim\tan(45°)$	10%
Z_3:	γ (kN/m³)	Normal	$15\sim20$	10%
Z_4:	q (kN/m²)	Lognormal	0 or $0.6\mu_\gamma$	30%
Z_5:	U		Samples drawn $f(u|D)$	

Selection of Prior PDFs for Random Variables

Table 3 summarizes the assumed prior PDF types, mean values (μ) and COV for the random variables in a typical design: $\tan(\phi)$ is taken to be normal with mean value $\mu_{\tan\phi}$ and 10% COV, and $\tan(\phi_f)$ is taken to be normal with mean value $\mu_{\tan\phi f}$ and 10% COV The unit weight γ is taken to be normal with mean value μ_γ and 10% COV The 10% COV is according to Phoon (1995) for the inherent variability of friction angle and unit weight. Traffic load q is taken to be lognormally distributed with mean value (μ_q) of 0 if traffic load is not considered (e.g., wall is designed for aesthetic purposes) and of $0.6\mu_\gamma$ kN/m² if traffic load is considered [e.g., wall will open for public traffic: using Eq. (2)]. The COV of q is taken to be 30% to model larger variability in traffic load.

Spatial variability of soil properties is not taken into account, i.e., the soil is assumed homogeneous. The impact of spatial vari-ability to the magnitude of earth pressure can be fairly complicated, as illustrated by Fenton et al. (2005) on a cantilever wall. Their conclusion is that the worst case happens when the scale of fluctuation is on the same order of the wall height. Therefore, the most conservative design approach is to assume the scale of fluctuation to be on the same order of wall height. In the writers' case, the scale of fluctuation is assumed to be very large (homogenous). This is definitely not the most conservative assumption. However, this homogeneous assumption prohibits the averaging effect, which in general will reduce the variability of the earth pressure. In this regard, the homogeneous assumption is conservative. In conclusion, the homogeneous assumption should be relatively conservative, although not the most conservative one.

For the scaling parameter U, it is necessary to obtain the samples from the posterior PDF $f(u|D)$. Fig. 9 demonstrates the posterior PDFs in a graphical way for various levels of friction angle vari-ability. The Metropolis algorithm (Metropolis et al. 1953) is adopted to obtain samples from these posterior PDFs.

Design Variables θ

In this study, the design variables θ include the aspect ratio L/H (θ_1), wall height H (θ_2), mean value of backfill friction angle $\mu_{\tan\phi}$ (θ_3), mean value of foundation friction angle $\mu_{\tan\phi f}$ (θ_4), mean value of unit weight μ_γ (θ_5), and mean value of traffic load μ_q (θ_6). According to practical design for MSE walls, the range of
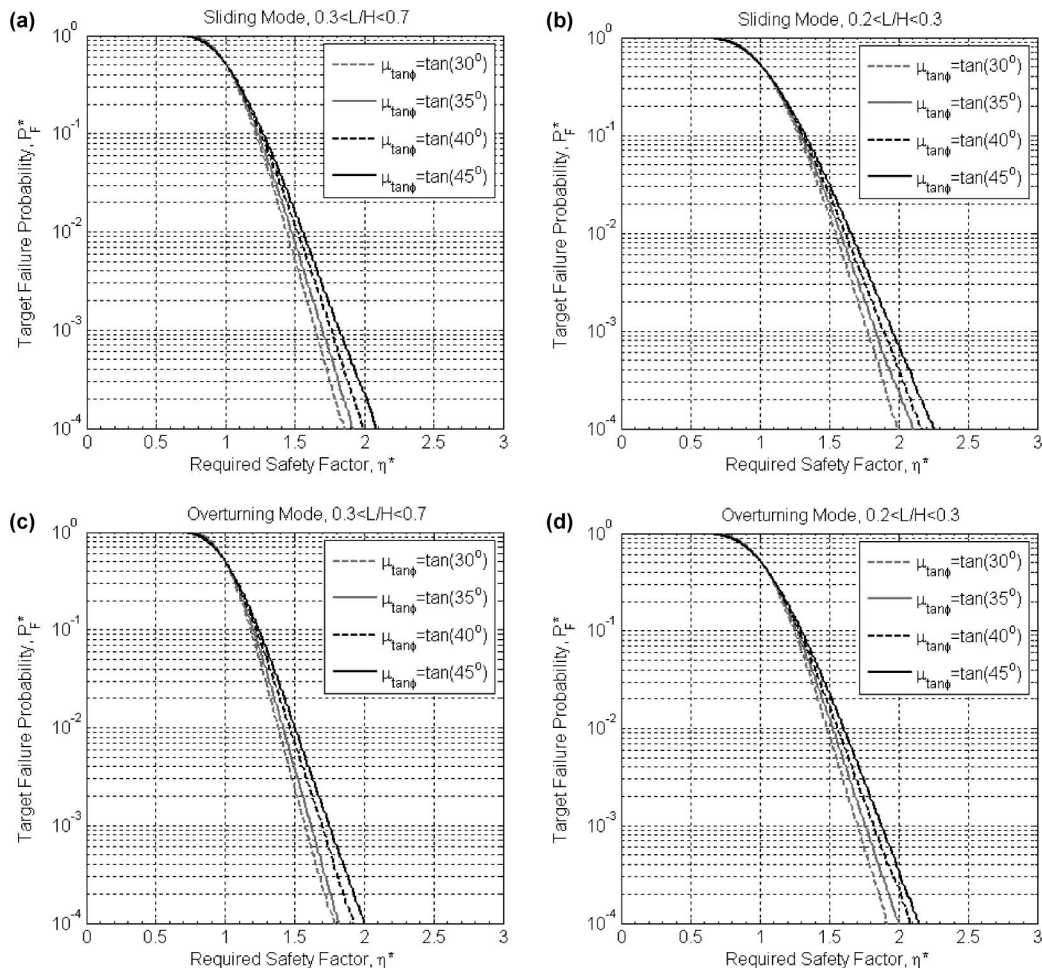

Fig. 11. Variation of η^* versus P_F^* relations over L/H: (a) sliding mode, $0.3 < L/H < 0.7$; (b) sliding mode, $0.2 < L/H < 0.3$; (c) overturning mode, $0.3 < L/H < 0.7$; (d) sliding mode, $0.2 < L/H < 0.3$

design variables is selected as $L/H \in [0.2\text{–}0.7]$, $H \in [3\text{ m–}9\text{ m}]$, $\mu_{\tan\phi} \in [\tan(30°)\text{–}\tan(45°)]$, $\mu_{\tan\phi f} \in [\tan(30°)\text{–}\tan(45°)]$, $\mu_\gamma \in [15\text{ kN/m}^3\text{–}20\text{ kN/m}^3]$, and $\mu_q = 0$ or $0.6\mu_\gamma$ kN/m².

Although Woodruff (2003) observed that external failure mainly happened when $L/H < 0.25$ for centrifuge tests, this observation only indicates that for narrow walls with $L/H < 0.25$, the probability of external instability is very high (almost certain). It does not imply narrow walls with $L/H > 0.25$ have "zero" probability of external instability. Therefore, in the sense of RBD, it is still important to evaluate the external stability of walls with $L/H > 0.25$. This is the reason for selecting L/H from 0.2–0.7 in this study.

For a realistic design process, engineers often need to iterate the design variables θ to reach the optimal design. For the RBD approach, it is therefore desirable to establish η^* versus P_F^* relations that are invariant over various choices of θ. Most design variables are found to have only slight influence on the η^* versus P_F^* relation because of the cancellation between $\overline{SR}(\theta)$ and $SR(Z,\theta)$. Specifically, μ_γ and $\mu_{\tan\phi f}$ have insignificant influence on η^* versus P_F^* relations because of nearly perfect cancellation in the division between $\overline{SR}(\theta)$ and $SR(Z,\theta)$. The variations of the η^* versus P_F^* relation with design variables other than μ_γ and $\mu_{\tan\phi f}$ in their practical ranges will be illustrated in the next section.

Last, the η^* versus P_F^* relations in general depends on the posterior PDF $f(u|D)$, which is affected by the assumed COV level for $\tan(\phi_{CF})$, as indicated in Fig. 9. However, it is found that the

calibrated η^* versus P_F^* relation does not change much for various posterior PDFs $f(u|D)$ in Fig. 9; therefore, only the posterior PDF $f(u|D)$ corresponding to 10% COV of $\tan(\phi_{CF})$ is taken for the subsequent presentation.

Main Results

A series of calibrated η^* versus P_F^* relations for sliding and overturning modes are presented in this section. The application of these η^* versus P_F^* relations for RBD designs will be illustrated by a design example in the next section. Figs. 11 and 12 present the variations of η^* versus P_F^* relations with wall aspect ratio L/H and wall height H, respectively, when traffic load is considered. The η^* versus P_F^* relation is slightly affected by $\mu_{\tan\phi}$, so this sensitivity is also shown in the figures. In Fig. 11, the η^* versus P_F^* relation is nearly invariant over L/H for $L/H > 0.3$; however, the η^* versus P_F^* relations start to slightly shift for $L/H < 0.3$. In developing Fig. 12, L/H is assumed to be greater than 0.3. In Fig. 12, the η^* versus P_F^* relation is nearly invariant over H, although H has a larger influence in the overturning mode. Fig. 13 presents the variations of η^* versus P_F^* relations with mean value of traffic load μ_q. Similar to Fig. 12, μ_q has a larger influence in the overturning mode.
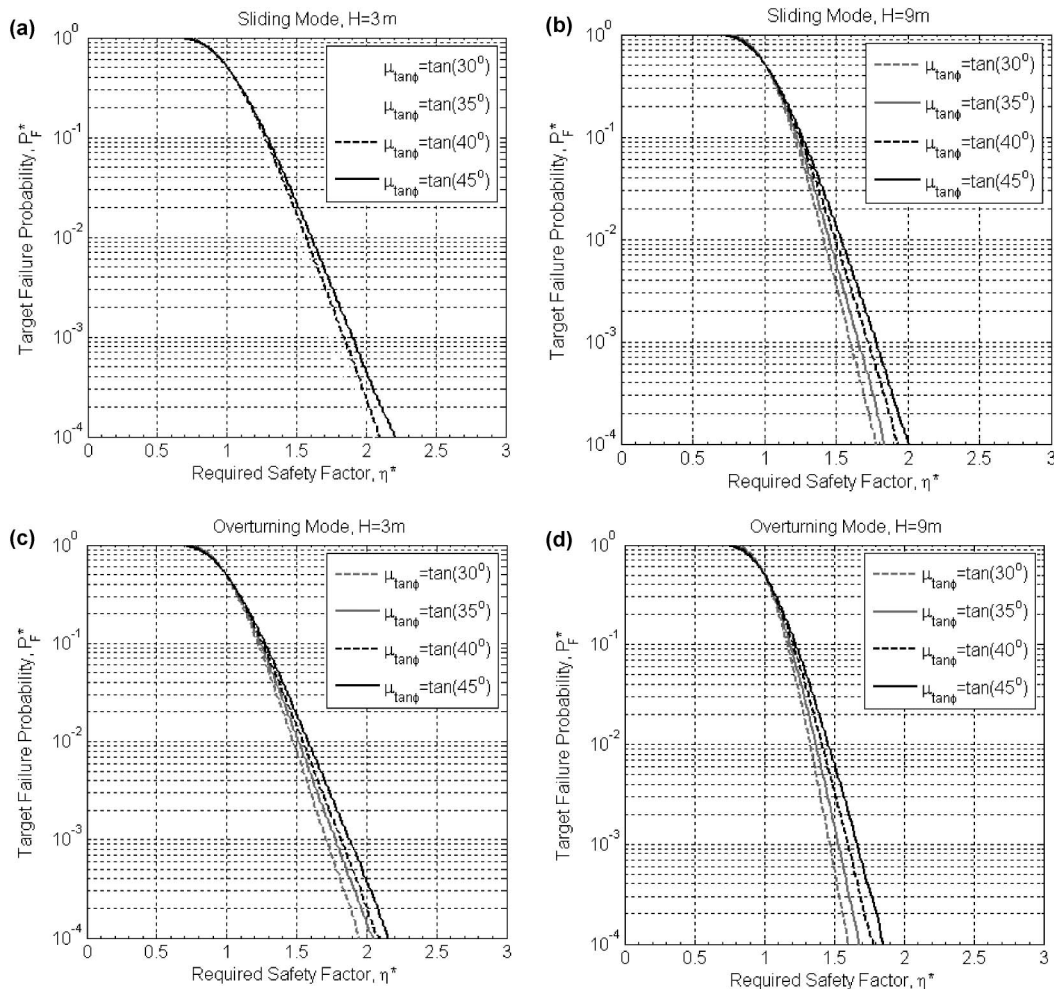

Fig. 12. Variation of η^* versus P_F^* relations over H: (a) sliding mode, $H = 3$ m; (b) sliding mode, $H = 9$ m; (c) overturning mode, $H = 3$ m; (d) sliding mode, $H = 9$ m
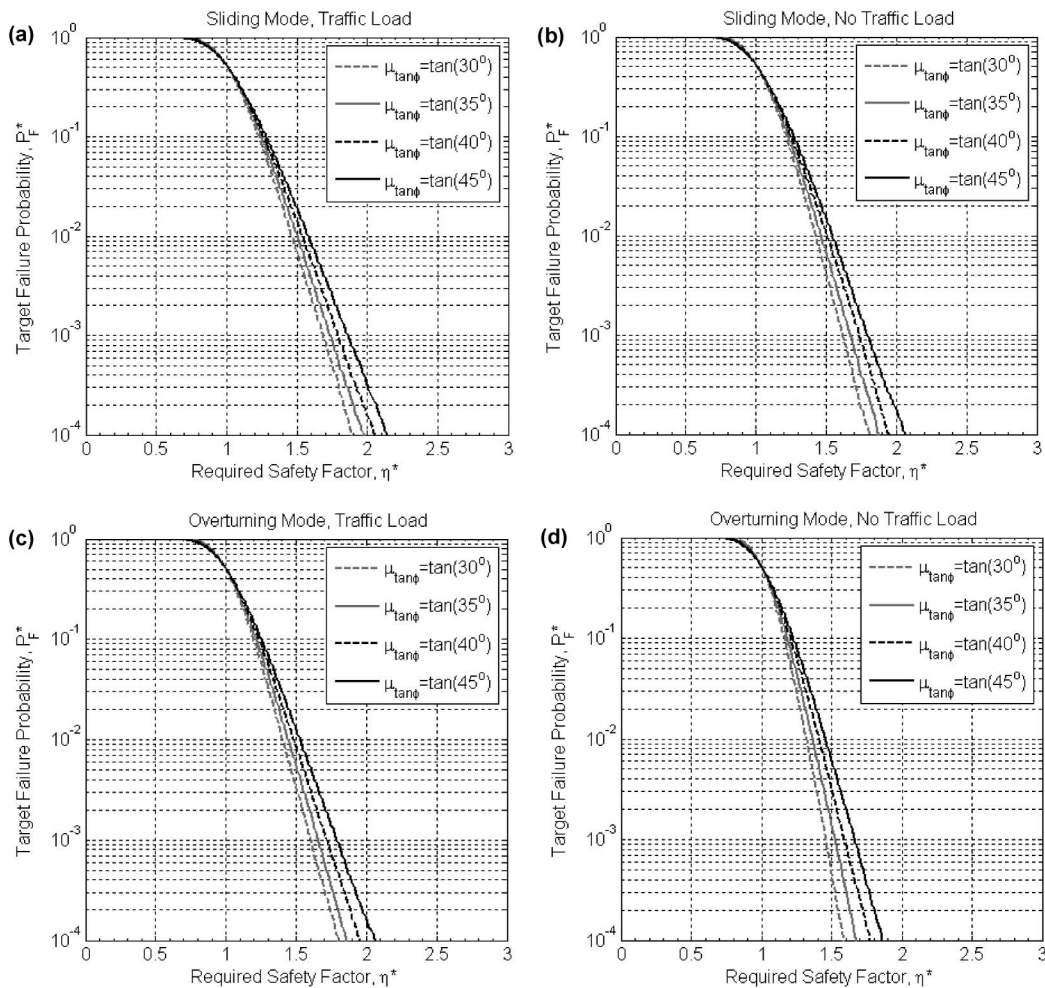
Fig. 13. Variation of η^* versus P_F^* relations over μ_q: (a) sliding mode, traffic load; (b) sliding mode, no traffic load; (c) overturning mode, traffic load; (d) sliding mode, no traffic load
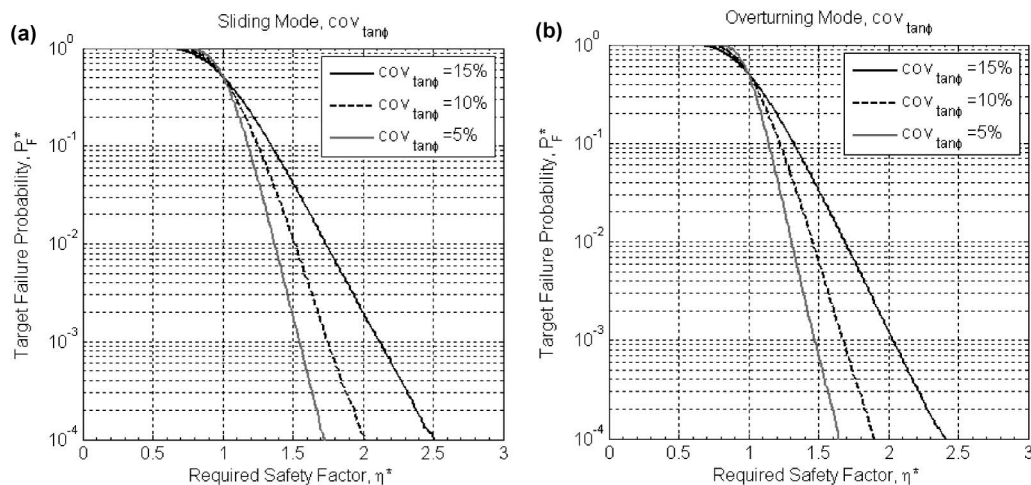

Fig. 14. Effect of COV of $\tan(\phi)$ when traffic load is considered: (a) sliding mode; (b) overturning mode

When extra evidence, e.g., detailed site investigation, indicates that the assumed COVs for the random variables Z are inappropriate, the 10% COV for $\tan(\phi)$ and unit weight as well as the 30% COV for traffic load should be replaced. Sensitivity analysis shows that the COV of $\tan(\phi)$ has a major effect on the calibrated η^* versus P_F^* relation, while the effect of the COV for traffic load and unit weight is negligible. Fig. 14 shows the η^* versus P_F^* relations for $\tan(\phi)$ COV $\in [5\%–15\%]$ when traffic load is considered, while Fig. 15 shows the results for zero traffic load. Since the COV of $\tan(\phi)$ significantly affects the η^* versus P_F^* relations, careful assessment of the COV of $\tan(\phi)$ is crucial.
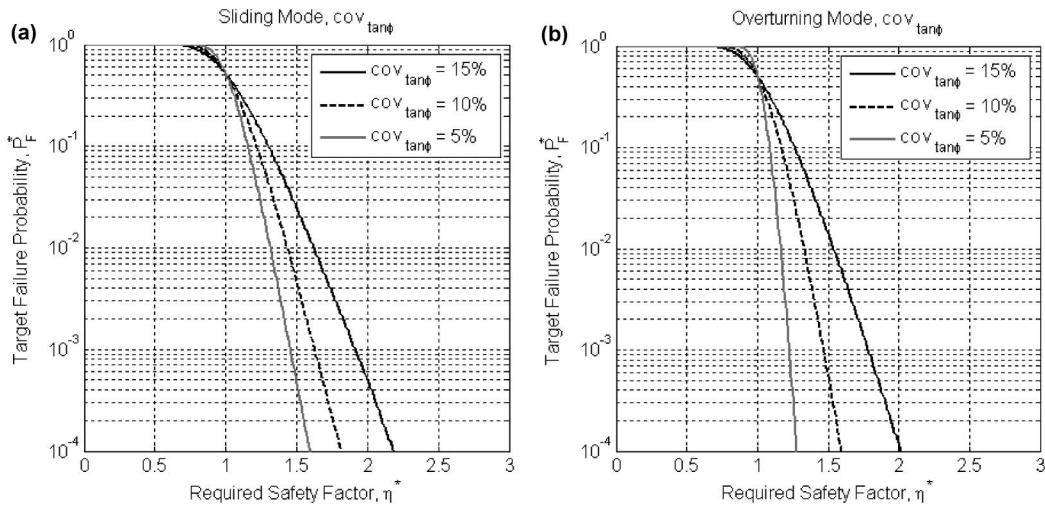
Fig. 15. Effect of COV of $\tan(\phi)$ when traffic load is not considered: (a) sliding mode; (b) overturning mode

Design Example

The following hypothetical example is taken to illustrate using the design charts (Figs. 11–15) for RBD.

A construction project plans to widen an existing highway to accommodate increasing traffic volume. The final decision of this project is to place a MSE wall in front of the stable face of the existing structure that has a height of 6 m. The tentatively selected backfill has an average friction angle of 40° and mean unit weight of 17 kN/m³. The foundation soil has an average friction angle of 40°. The target failure probability for permanent geotechnical structure is 0.001 selected from FHwA geotechnical risk-analysis guidelines (Baecher 1987). What is the minimum value of wall aspect ratio for the failure probability to satisfy the above criterion for both sliding and overturning modes?
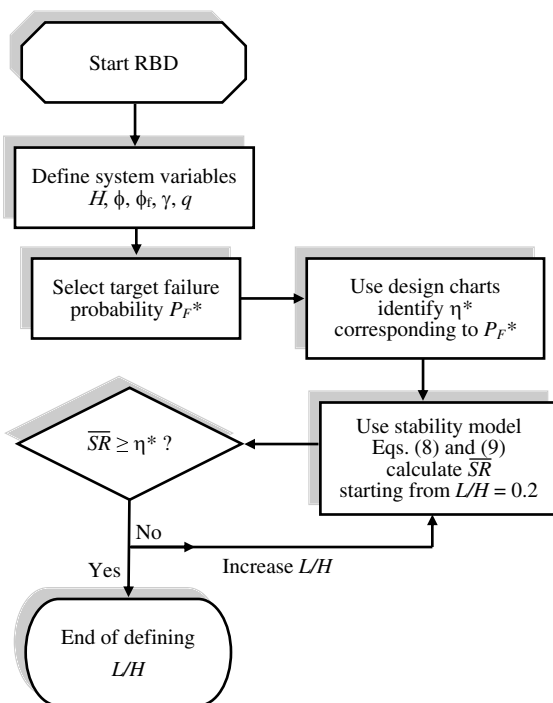

Fig. 16. Flowchart for the proposed design procedure

The procedure for the preceding design example can be addressed using the steps shown in the flowchart in Fig. 16. The key components are presented as follows:

1. The design variables $H = 6$ m, $\mu_{\tan \phi} = \tan(40°)$, $\mu_{\tan \phi f} = \tan(40°)$, and $\mu_\gamma = 17$ kN/m³ should be considered fixed and cannot be altered by the designer unless a decision is made to replace the soils. The traffic load should be considered in the design because this MSE wall opens to public traffic, hence $\mu_q = 0.6\mu_\gamma$. The COVs of $\tan(\phi)$, $\tan(\phi_f)$, and γ are assumed to be a typical value of 10%. The COV of q is assumed to be 30% for a larger variability in traffic load. The only design variable subjected to a design decision is L/H.

2. Select η^* corresponding to the target failure probability: The RBD criterion is $P_F^* < 0.001$ for both sliding and overturning modes. Recall that the influence of $\mu_{\tan \phi f}$ and μ_γ to the η^* versus P_F^* relation is insignificant. Also, the influence of L/H is insignificant as long as $L/H > 0.3$. First assume that the final decision is to let $L/H > 0.3$. Based on this assumption, Fig. 12 can be used to find the required nominal safety ratio η^* for both failure modes. However, Fig. 12 only shows the η^* versus P_F^* relations for $H = 3$ m and 9 m. The following steps are therefore taken to estimate η^* corresponding to $P_F^* = 0.001$: find the η^* corresponding to $P_F^* = 0.001$ for $H = 3$ m and 9 m for both failure modes (use the curves for $\mu_{\tan \phi} = 40°$ in Fig. 12). This will give two η^* values for each failure mode, one for $H = 3$ m and the other for $H = 9$ m. Averaging the two values will give a good estimate for the η^* value for $H = 6$ m. The corresponding η^* is approximately 1.75 for sliding and 1.65 for overturning.

3. Determine minimum value of L/H: The required nominal safety ratio η^* (i.e., 1.75 or 1.65) serves as the smallest nominal safety ratios $\overline{SR}$ necessary for the RBD design. Since the nominal safety ratios $\overline{SR}$ can be calculated using Eqs. (8) and (9), one needs to select a minimum value of L/H so that the resulting $\overline{SR}_s$ will be larger than 1.75 and $\overline{SR}_o$ will be larger than 1.65. It is worthwhile to remind one that the definition of $\overline{SR}_s$ and $\overline{SR}_o$ is different from the conventional safety factors: the difference is in the term $1/(1 - \overline{F})$. The minimum value of L/H can be determined by starting with $L/H = 0.2$ and increasing this value until $\overline{SR} \geq \eta^*$. In this example, the minimum value of L/H is found to be 0.44 and 0.39 for the

sliding mode and overturning mode, respectively. Therefore, $L/H = 0.44$ should be taken.

4. Verification (optional): This design scenario of $L/H = 0.44$ is further verified by Monte Carlo simulation with one million samples, which shows that the failure probability for $L/H = 0.44$ is 8×10^{-4} for sliding and 4×10^{-6} for overturning.

It is instructive to know how the FHwA MSE-wall design guidelines (Elias et al. 2001) compares with the proposed design charts. In the guidelines, the conventional safety factor [i.e., Eqs. (8) and (9) for $\bar{F} = 0$] is required to be 1.5 for sliding and 2.0 for overturning. The minimum value of L/H can also be determined by using the conventional safety-factor requirements. The minimum value of L/H is 0.39 for sliding and 0.43 for overturning. As a result, $L/H = 0.43$ should be taken. By using Fig. 12 and recognizing that there is a $1/(1 - \bar{F})$ ratio of difference between $\overline{SR}$ and the conventional safety factor, it is concluded that the FHwA MSE-wall design guidelines correspond to $P_F^* = 0.006$ for sliding and $P_F^* = 0.0001$ for overturning.

Conclusions

This paper studies the external stability of narrow MSE walls. A stability model is proposed to calculate the stability against sliding and overturning. The effect of reduced earth pressure, an important characteristic of narrow MSE walls, is included in the proposed stability model. The variability in the reduction factor that characterizes model uncertainties is calibrated by centrifuge test data. The main improvements over conventional works include a better capture of reduced earth pressure by introducing a reduction factor and design charts for RBD. The following conclusions are drawn from this study.

- Design charts representing the relation between target reliability and required nominal safety ratio are provided for practical use. The benefit of the relation is that one can achieve a RBD by using the safety-factor approach, and the required safety factor can be easily found from the charts. Readers should also notice that a good design practice is assumed in this study (i.e. no accumulation of water pressure within MSE walls); therefore, the proposed design charts may not be applicable to designing MSE walls when the consideration of water pressure is required.
- The bearing capacity failure mode is not calibrated in this study because of the calibration limitation using centrifuge test results. Yet, based on noncalibrated simulations, for MSE walls with L/H greater than 0.35, the failure probability for this mode is usually less than 0.01. For walls with L/H less than 0.35, it is advisable that the bearing capacity mode should be carefully assessed.
- It is worth mentioning that Fenton et al. (2005) studied the effects of correlation length over the reliability of cantilever retaining walls. Such effects are not taken into account, i.e., the soil is assumed homogeneous. The impact of spatial variability to the magnitude of earth pressure can be fairly complicated, as illustrated by Fenton et al. (2005) on a cantilever wall. Their conclusion is that the worst case happens when the scale of fluctuation is in the same order of the wall height. Therefore, the most conservative design approach is to assume the scale of fluctuation to be in the same order of wall height. In the writers' case, the scale of fluctuation is assumed to be very large (homogenous). This is definitely not the most conservative assumption. However, this homogeneous assumption prohibits the averaging effect, which in general will reduce the variability of the earth pressure. In this regard, the homogeneous assumption is conservative. In conclusion, the homogeneous assumption

should be relatively conservative, although not the most conservative one.

Appendix: Relationships between η^* and P_F^*

In this appendix, a theorem is reviewed to illustrate the relation between the target failure probability P_F^* and the required safety factor η^*. This theorem follows from a theorem originally proposed by Ching (2009). In terms of RBD, the design target is to ensure the chosen design will meet certain failure probability requirements as in Eq. (17):

$$P(SR(Z, \theta) < 1 | \theta, D) \leq P_F^* \qquad (17)$$

where P_F^* = target failure probability; Z contains all random variables (including tangent of backfill friction angle ϕ, tangent of foundation friction angle ϕ_f, unit weight γ, traffic load q and scaling parameter U); θ contains parameters of chosen design variables (including the aspect ratio L/H, wall height H, mean value of traffic load μ_q, mean value of tangent of backfill friction angle $\mu_{\tan \phi}$, mean value of tangent of foundation friction angle $\mu_{\tan \phi f}$, and mean value of unit weight μ_γ); D = Woodruff's centrifuge test data. The centrifuge test information is conveyed through the conditioning on D. Ching (2009) shows that RBD in Eq. (17) is equivalent to the following safety-factor design:

$$\overline{SR}(\theta) \geq \eta^* \qquad (18)$$

where η^* = required safety factor to meet the target failure probability. The functional relationships between η^* and P_F^* are shown in Eq. (19):

$$P(\overline{SR}(\theta)/SR(Z, \theta) > \eta^* | \theta, D) = P_F^* \qquad (19)$$

For ease of presentation, $\overline{SR}(\theta)/SR(Z, \theta)$ will from now on be denoted by $G(Z, \theta)$.

To implement this theorem, the relation between η^* and P_F^* is first determined from Eq. (19). Once this relation is obtained, the required safety factor corresponding to a prescribed target failure probability can be identified. According to the theorem, a design
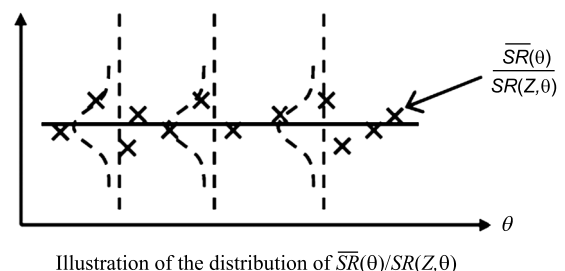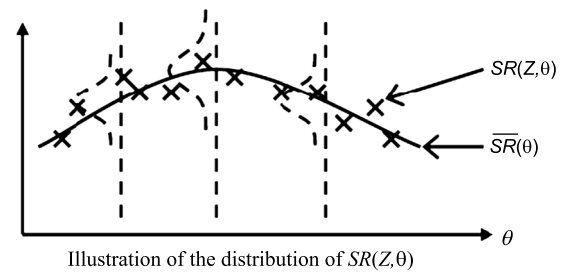

Illustration of the distribution of $SR(Z, \theta)$

Illustration of the distribution of $\overline{SR}(\theta)/SR(Z, \theta)$

Fig. 17. Illustration of the distribution of $SR(Z, \theta)$ and $\overline{SR}(\theta)/SR(Z, \theta)$

satisfying the safety-factor criterion will also satisfy the target reliability, i.e., RBD can be achieved through a safety-factor design.

Although the theorem seems nontrivial, a simplified procedure based on MCS can be used to estimate the η^* versus P_F^* relations: draw N samples of Z, denoted by $\{Z^{(i)}: i = 1, \ldots, N\}$, where Z samples are drawn from the PDF of Z conditioning on the centrifuge data D. Let $G^{(i)} = G(Z^{(i)}, \theta)$. At the end of MCS, $\{G^{(i)}: i = 1, \ldots, N\}$ is obtained. For a chosen η^* value, the corresponding P_F^* value can be easily estimated by the law of large numbers in Eq. (20):

$$P_F^* \approx \frac{1}{N}\sum_{i=1}^{N} I(G^{(i)} > \eta^*) \qquad (20)$$

By changing the η^* value, one can estimate the corresponding P_F^* values by repetitively applying Eq. (20); the entire functional relation between η^* and P_F^* is then obtained. In the current study, one million samples ($N = 10^6$) are taken to establish the η^* versus P_F^* relations for both sliding and overturning modes. It is essential to obtain Z samples conditioning on the centrifuge data D. By doing this, the so-determined η^* versus P_F^* relation will "absorb" the information contained in the centrifuge tests. The equivalence between Eqs. (17) and (18) is only for a fixed value of θ, not for a range of θ. In fact, from Eq. (19) it is clear that the calibrated η^* versus P_F^* relation in general will change with θ. In other words, the calibrated η^* should depend on θ. However, it turns out the η^* versus P_F^* relation usually does not change dramatically for a range of possible θ values. This is because the probability distribution of $\overline{SR}(\theta)/SR(Z, \theta)$ usually does not change much with θ owing to the cancellation between $\overline{SR}(\theta)$ and $SR(Z, \theta)$ in division: when θ is varying, $\overline{SR}(\theta)$ and $SR(Z, \theta)$ either increase or decrease in a similar pattern. The concept of the cancellation between $\overline{SR}(\theta)$ and $SR(Z, \theta)$ is illustrated in Fig. 17. The cancellation in $\overline{SR}(\theta)/SR(Z, \theta)$ implies that the probability $P(\overline{SR}(\theta)/SR(Z, \theta) > \eta^*|\theta, D)$ and consequently the η^* versus P_F^* relation may not vary drastically over θ.
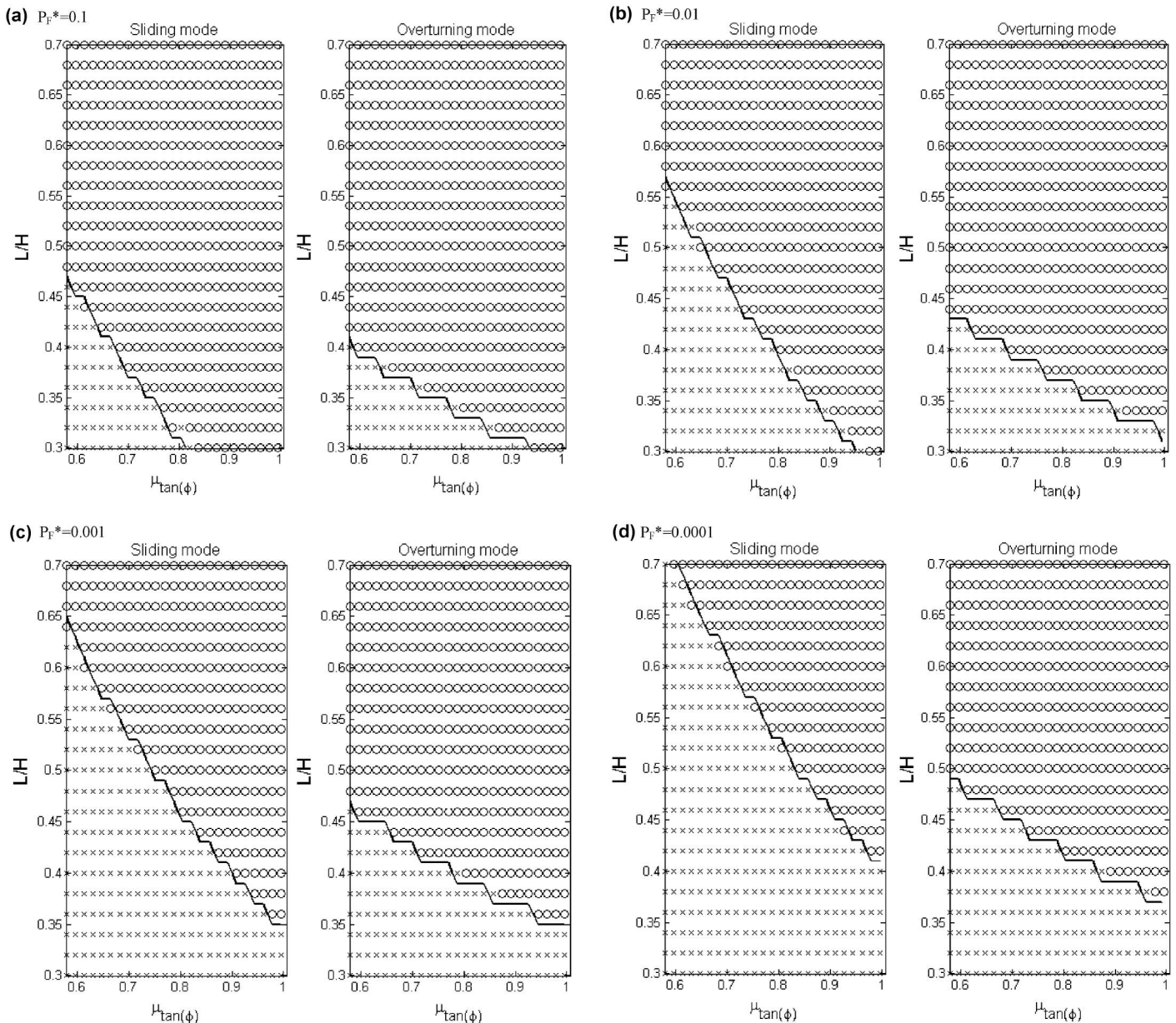

Fig. 18. Results for sliding and overturning modes: (a) $P_F^* = 0.1$; (b) $P_F^* = 0.01$; (c) $P_F^* = 0.001$; (d) $P_F^* = 0.0001$. The "X" region is the region where P_F is larger than P_F^*, while the "○" region is the region where P_F is less than P_F^*. The shaded region is the region of $\eta^* \overline{SR}(\theta) \leq 1$

One way to justify the preceding cancellation is to find the η^* versus P_F^* relation for various θ to see whether the relation changes mildly with changing θ. Another equivalent way to justify the cancellation is to check if the allowable RBD set $\sum_R = \{\theta: P(SR[Z, \theta] > 1.0|\theta) \leq P_F^*\}$ is indeed close to the allowable safety-factor set $\sum_S = \{\theta: \overline{SR}(\theta) \geq \eta^*\}$ for all $[\eta^*, P_F^*]$ pairs satisfying Eq. (19). The latter way for the verification is carried out through a series of MCSs. The comparison between the allowable RBD and safety-factor sets should, in principle, be made in the θ space, a six-dimensional space of L/H, H, μ_q, $\mu_{\tan\phi}$, $\mu_{\tan\phi f}$, and μ_γ. For brevity, only the comparison for the case considering traffic load (i.e., μ_q is fixed at $0.6\mu_\gamma$ kN/m^2), $\mu_\gamma = 18$ kN/m^3, $\mu_{\tan\phi f} = \tan(40°)$, and $H = 6$ m is presented. Therefore, the comparison will be made in the two-dimensional space of $\mu_{\tan\phi}$ and L/H. The verifications on other scenarios show similar conclusions and will not be presented.

In the design region of $\mu_{\tan\phi}$ and L/H, each of the coordinate axes is divided into discrete points, creating grid points in specified design regions: $\mu_{\tan\phi} \in [\tan(30°), \tan(45°)]$ and $L/H \in [0.3\text{--}0.7]$ with small intervals. A total of $525 = 25 \times 21$ grid points represent 525 different design scenarios of $\mu_{\tan\phi}$ and L/H. The actual failure probability of each grid point (or design scenario) is evaluated by a set of MCSs with one million samples. Fig. 18 shows the results for given target failure probabilities $P_F^* = 0.1, 0.01, 0.001,$ and 0.0001, respectively. If the actual failure probability at a grid point is less than P_F^*, it is marked as an open circle "○"; otherwise, it is marked as an "X." Therefore, the region occupied by the open circle "○" should be close to the allowable RBD set $\sum_R = \{\theta: P(SR[Z, \theta] > 1.0|\theta) \leq P_F^*\}$. On the other hand, for given P_F^*, the corresponding η^* is identified from Figs. 11–15 and the allowable safety-factor design set $\sum_S = \{\theta: \overline{SR}(\theta) \geq \eta^*\}$ is plotted as the shaded region. The η^* versus P_F^* relation is verified if all "X" are outside the blue shadow and all "○" are inside the blue shadow. As shown in Fig. 18, the comparisons seem satisfactory; only slight mismatch occurs at the boundary between shaded and unshaded regions. This slight mismatch is attributed to the imperfect cancellation between $\overline{SR}(\theta)$ and $SR(Z, \theta)$.

In conclusion, the comparison shows that the design charts in Figs. 11–15 are consistent to the results from MCS. Fig. 18 is only for the purpose of validation. Once the validation is satisfactory, Figs. 11–15 can be directly used for practical designs without further verifications.

References

AASHTO. (2002). "Standard specifications for highway bridges." *HB-17*, 7th Ed., Washington, DC.

ASTM. (2009). "Standard test method for tensile properties of geotextiles by the wide-width strip method." *D4595-09*, West Conshohocken, PA.

Baecher, G. H. (1987). "Geotechnical risk analysis user's guide." *Rep. No. FHwA-RD-87-011*, Federal Highway Administration, Washington, DC.

Chalermyanont, T., and Benson, C. H. (2004). "Reliability-based design for internal stability of mechanically stabilized earth walls." *J. Geotech. Geoenviron. Eng.*, 130(2), 163–173.

Chalermyanont, T., and Benson, C. H. (2005). "Reliability-based design for external stability of mechanically stabilized earth walls." *Int. J. Geomech.*, 5(3), 196–205.

Ching, J. (2009). "Equivalence between reliability and factor of safety." *Probabilistic Eng. Mechanics*, 24(2), 159–171.

Elias, V., Christopher, B. R., and Berg, R. R. (2001). "Mechanically stabilized earth walls and reinforced soil slopes design and construction guidelines" *Rep. No. FHwA-NHI-00-043*, National Highway Institute, Federal Highway Administration, Washington, DC.

Fenton, G. A., Griffiths, D. V., and Williams, M. B. (2005). "Reliability of traditional retaining wall design." *Geotechnique*, 55(1), 55–62.

Filz, G. M., and Duncan, J. M. (1997a). "Vertical shear loads on nonmoving walls. I: Theory." *J. Geotech. Geoenviron. Eng.*, 123(9), 856–862.

Filz, G. M., and Duncan, J. M. (1997b). "Vertical shear loads on nonmoving walls. II: Application." *J. Geotech. Geoenviron. Eng.*, 123(9), 863–873.

Frydman, S., and Keissar, I. (1987). "Earth pressure on retaining walls near rock faces." *J. Geotech. Eng.*, 113(6), 586–599.

Handy, R. L. (1985). "The arc in soil arching." *J. Geotech. Eng.*, 111(3), 302–318.

Kniss, K. T., Yang, K.-H., Wright, S. G., and Zornberg, J. G. (2007). "Earth pressures and design consideration of narrow MSE wall." *Proc. Texas Section ASCE Spring 2007*, ASCE, Reston, VA.

Lawson, C. R., and Yee, T. W. (2005). "Reinforced soil retaining walls with constrained reinforced fill zones." *Proc., GeoFrontiers 2005*, ASCE, Reston, VA, 2721–2734.

Leshchinsky, D., Hu, Y., and Han, J. (2004). "Limited reinforced space in segmental retaining wall," *Geotext. Geomembr.*, 22(6), 543–553.

Metropolis, N., Rosenbluth, A. E., Rosenbluth, M. N., Teller, A. H., and Teller, E. (1953). "Equation of state calculations by fast computing machines." *J. Chem. Phys.*, 21, 1087–1092.

Morrison, K. F., Harrison, F. E., Collin, J. G., Dodds, A., and Arndt, B. (2006). "Shored mechanically stabilized earth (SMSE) wall systems design guidelines." *Rep. No.FHwA-CFL/TD-06-001*, Federal Highway Administration, Central Federal Lands Highway Division, Washington, DC.

Phoon, K. (1995). "Reliability-based design of foundations for transmission line structures." Ph.D. dissertation, Cornell Univ., Cornell, NY.

Take, W., and Valsangkar, A. (2001). "Earth pressures on unyielding retaining walls of narrow backfill width."*Can. Geotech. J.*, 38(6), 1220–1230.

Woodruff, R. (2003). "Centrifuge modeling of MSE-shoring composite walls." Master thesis, Univ. of Colorado, Boulder, CO.

Yang, K.-H., Kniss, K. K., Zornberg, J. G., and Wright, S. G. (2008). "Finite-element analyses for centrifuge modeling of narrow MSE walls." *Proc., First Pan American Geosynthetics Conference, GEOA-MERICAS-2008* (CD-ROM), International Fabrics Association Int., Roseville, MN, 1246–1255.

Yang, K.-H., and Liu, C.-N. (2007). "Finite-element analysis of earth pressures for narrow retaining walls." *J. GeoEng.*, 2(2), 43–52.

Zornberg, J. G. (2002). "Peak versus residual shear strength in geosynthetic-reinforced soil design." *Geosyn. Int.*, 9(4), 301–318.